RESEARCH ARTICLE

Journal of **RAMAN SPECTROSCOPY** WILEY

SEM/Raman spectroscopy of clathrites as analogs of authigenic carbonates in ocean worlds

Ana de Dios-Cubillas[1,2] ⊕ | **Olga Prieto-Ballesteros**[1] | **Manfred Nachtnebel**[3] | **Harald Fitzek**[3] | **Hartmuth Schröttner**[3,4]

[1]Centro de Astrobiología (CAB), CSIC-INTA, Torrejón de Ardoz, Madrid, Spain

[2]Departamento de Biología, Geología, Física y Química Inorgánica, Universidad Rey Juan Carlos, Calle Tulipán s/n, Móstoles, Madrid, Spain

[3]Graz Centre for Electron Microscopy (ZFE), Graz, Austria

[4]Institute of Electron Microscopy and Nanoanalysis (FELMI), Graz University of Technology, Graz, Austria

Correspondence
Ana de Dios-Cubillas and Olga Prieto-Ballesteros, Centro de Astrobiología (CAB), CSIC-INTA, Carretera de Ajalvir km 4, Torrejón de Ardoz, Madrid, 28850, Spain.
Email: adedios@cab.inta-csic.es and prietobo@cab.inta-csic.es

Abstract

There is evidence from the near-infrared observations of space missions of the presence of carbonates on the surface of several ocean worlds. However, their genesis remains unresolved. We investigate the hypothesis that these carbonates may be in the form of clathrites assuming that clathrate hydrates are stable phases in the crust and ocean of these ocean worlds. In order to support this, we studied a sample of a potential clathrite from the Hydrate Ridge cold seep (Cascadia Subduction Zone), the carbonate rock fossil of clathrate hydrates, as a terrestrial analogue. We characterised the mineralogy and texture of the sample by using a coupled confocal Raman microscope and scanning electron microscopy instrument with the aim of identifying possible geo- and biosignatures, which could be relevant for future missions of exploration to ocean worlds and Mars. Our results show that aragonite is the dominant mineral phase in the clathrite sample, but Mg-calcite and dolomite were also identified. These three carbonates constitute a pattern related to clathrate hydrate formation and dissociation processes. Dolomite was defined as a biosignature of gas hydrate microbiomes because it was integrated within Mg-calcite grains precipitated after clathrate hydrate dissociation. Nevertheless, no spectral changes were observed in Raman bands of carbonate minerals that would indicate the influence of clathrate hydrates in their genesis. We also observed that Raman band positions of the associated framboidal pyrites are a characteristic signature of the associated framboid-like texture because its potential as biosignature may only be attributed by biochemical analysis.

KEYWORDS

clathrite, clathrate hydrates, ocean worlds, Raman, SEM

1 | INTRODUCTION

Clathrites are carbon-bearing gas-derived authigenic carbonate rocks. The root of the word 'clathr-ite' refers to its genesis, which means that clathrites are result of the formation and dissociation of clathrate hydrates.[1,2] Clathrate hydrates are defined as water ice minerals that retain gas molecules within their crystalline structure.[3] Thus, the defining characteristic of clathrites is that their carbonate ions come from carbon species of the dissociated clathrate hydrates.[2]

Identification of clathrites is currently constrained to planet Earth. However, there are two main lines of evidence that suggest that clathrites might also be present in the ocean worlds of the outer solar system. First, geophysical models support the presence of clathrate hydrates in the icy crust and ocean of Jupiter's moon Europa,[4] Saturn's moon Enceladus[5] and the dwarf planet Ceres,[6] among others. These presence of these clathrate hydrates would provide thermal insulation to the oceans due to their low thermal conductivity[7] and therefore help to explain some planetary geodynamic processes, such as cryomagmatic ascent resulting from clathrate hydrates dissociation that can culminate in the formation of particular surface features (i.e., from Europa's chaos terrains[8] to the gas injection processes that trigger the generation Enceladus' vents[5,9]). Second, evidence for the presence of carbonates within these ocean worlds comes also from the spectral signature of hydrated phases that potentially include carbonates on Ceres' bright spots (VNIR@Dawn),[10] Saturn's E-ring ice grains (CDA@Cassini),[11] and on low albedo regions from the Europa surface (NIMS@Galileo).[12] These planetary sites in which carbonates can be present would be linked to endogenous processes and material exchange from the underlying ocean or crustal liquid reservoirs to the surface. For example, Ceres' bright spots are associated to cryovolcanic and impact features,[10] Saturn's E-ring would be fed by Enceladus' surface vents,[13] and low albedo deposits of Europa have been described as materials emplaced on the surface that are the result of cryomagmatic processes.[14]

Clathrites are identified on Earth in geological contexts associated to material transfer processes involving aqueous environments. The formation of terrestrial clathrites takes place in cold-seep environments on the seafloor because it is in such locations where the high-pressure and low-temperature conditions for the formation and dissociation of clathrate hydrates occur.[15] In this case, the mobilised material that migrate upwards from the subsurface reservoir toward the seabed, which is susceptible to be enclathrated, consists of a fluid enriched in methane and other hydrocarbon compounds.[16] Clathrate hydrates are transitionally carbon sinks; therefore, upon dissociation, the carbon element of released gas molecules can be sequestrated again in the form of clathrites.[2]

Clathrites present a brecciated fabric resulting from sediment collapse associated with the dissociation of clathrate hydrates[16] and could be considered cement-supported, monomictic breccia. Clasts of sedimentary rocks are cemented by botryoidal aragonite and high-magnesium calcite[17] that precipitated in relation to varying concentrations of magnesium and sulphate[16,18] in pore-water during processes of clathrate hydrate formation and dissociation. Aragonite syn-precipitate to clathrate hydrates as they form, mimicking their sponge-like bubble crystal habit.[16,17] This particular morphology acquired by aragonite develops in the presence of clathrate hydrate-bearing cold seeps, which is the calcium carbonate polymorph favoured by the increasingly ionic content of the remaining pore-water resulting of the salting-out effect caused by the formation of clathrate hydrates.[18,19] Unlike aragonite, Mg-calcite precipitates after clathrate hydrate dissociation, inheriting their heavy oxygen isotopic composition given that the clathrate hydrate lattice is preferentially built from heavy water molecules.[17]

Cold-seeps are habitable environments for the so-called seep communities,[20] and thus, authigenic aragonite and Mg-calcite may be bio-mediated precipitates. Anaerobic oxidation of methane from dissociated clathrate hydrates or directly from deep reservoirs, produced by consortia of methanotrophic archaea and sulphate reducing bacteria, would contribute to increase alkalinity and to the precipitation of clathrites or authigenic carbonates[2,21–23] (for more comparative information on the different genetic types of carbonates in cold seeps, see Carrizo et al.[21]). Venting of carbon-gaseous compounds thereby marks the beginning of the biogeochemical carbon cycle in these environments. Oddly enough for life, clathrate hydrates would not represent final carbon sinks in their strict sense, but would host microhabitats. This happens when clathrate hydrates grow so rapid that generates massive deposits in which intercrystalline pore spaces can encapsulate the rejected organic-saline solutions, providing enclosed mediums that are rich in energy sources for microorganisms. Snyder et al.[24] reached this conclusion after discovering a spherulitic aggregate of microdolomite residue inside a massive clathrate hydrate deposit in Joetsu Basin (offshore Niigata, the Japan Sea), where these microdolomite residues were the bio-products of organotrophic metabolic pathways.

Authigenic carbonates from cold seeps are considered terrestrial analogues of some Martian carbonates based on remote sensing observations.[25] In recent years, the potential for habitability of the ocean worlds of the solar

system have made them a priority target for astrobiological studies and their study has intensified. This, together with the possible presence of carbonates in these ocean worlds,[10–12] put cold-seep environments and their associated authigenic carbonates in the spotlight also as terrestrial analogues for processes and environments that could be present in these ocean worlds. In this context, clathrites are important not only as a geosignature to identify fossil deposits of clathrate hydrates[26] but also as a biosignature-containing matrix[21,24] like textually distinctive carbonate minerals (aragonite, high Mg-calcite and microdolomite) that can correlated with specific carbon and oxygen isotopic ratios, lipid biomarkers evidencing the coupling between anaerobic oxidation of methane and bacterial sulphate reduction and microbial DNA.[2,17,21,24]

Raman spectroscopy has already proven its efficacy for the detection of geo- and biosignatures as those that may be associated to clathrate hydrates,[27] clathrate hydrate-associated carbonates[28] and other materials of astrobiological interest.[29,30] Within exploration rovers, Raman spectrometers are part of present and future rover payloads to explore Mars, such as those included in Mars2020 Perseverance (Sherloc and Supercam)[31] and the ExoMars Rosalind Franklin (Raman Laser Spectrometer, RLS),[27,32] and are being considered as baseline instruments for future missions to ocean worlds like Titan.[33] For this reason, the Raman characterisation of clathrites in the laboratory and their associated geo- and biosignatures is of critical importance as part as the support and preparation for these missions of astrobiological interest.

2 | MATERIALS AND METHODS

This study complements the previous mineralogical characterisation of the clathrite sample and the stable isotope

TABLE 1 Overview of results of the mineral and organic geochemistry of the clathrite sample published in Carrizo et al.[21]

Petrographic and mineralogical characterisation				
Clathrate hydrate breccia (angular clasts)				
Clasts	**Accesory minerals**	**Calcareous cement**		
Quartz, SiO_2	Opaque minerals (oxides, sulphides)	Aragonite, $CaCO_3$		
Chlorite-serpentine, $(Mg,Al)_6(Si,Al)_4O_{10}(OH)_8$	High-Mg calcite, $(Mg_{0.129},Ca_{0.871})CO_3$			
	Geochemical characterisation			
	TOC	**$\delta^{13}C_{org}$**	**$\delta^{13}C_{inorg}$**	**$\delta^{18}O$**
	9%	−49.1‰	−44.8‰	3.6‰
	Lipid characterisation			
	Lipid compounds ($\mu g \cdot g^{-1}$)	**Bulk isotopic composition (‰)**	**Biomarkers**	
	Crocetane	1.4	−105‰	Methanotrogenic and/or methanotrophic archaea
	PMI	0.98	−113‰	
	$isoC_{15:0}$	1.3	−84.4‰	Sulphate-reducing bacteria
	$anteisoC_{15:0}$	2.5	−87.6‰	
	$C_{16:1w7}$	3.6	−59.1‰	
	archaeol	11	−118‰	Archaeal anaerobic methanotrophs (ANME) of the clades ANME-1 and ANME-2
	sn-2-hydroxyarchaeol	3.6	−113‰	

and lipid biomarker analyses[20] performed on the carbonate fraction (Table 1) by correlative Scanning Electron Microscope (SEM)-Raman microscope at the FELMI-ZFE facility (Graz, Austria). We used SEM-EDS imaging to find candidate points for Raman measurements in order to evaluate potential geo- and biosignatures by identifying changes in the spectroscopic parameters (Raman band position, width, intensity ratio and area) and correlating them with organic-like or geometric mineral textures.

2.1 | Sample preparation

Clathrite sample (Figure 1A) was collected from the cold seep site at Hydrate Ridge (Cascadia Margin, Oregon coast, Figure 1B).[16,34] A 10 mm diameter piece of clathrite sample was cut so that it could be placed onto the microscope stage for SEM-Raman analysis (Figure 1C). The clathrite sample showed a slightly unconsolidated behaviour on the geological cutting machine; hence, it was necessary to embed it into a resin matrix.

2.2 | Raman Imaging and Scanning Electron Microscopy (RISE)

RISE is a WITec confocal Raman microscope that is fully integrated into a Zeiss Sigma 300 VP SEM coupled with an Oxford SSD X-Max 80 Energy-Dispersive X-Ray Spectroscope (EDXS). Both Raman and SEM are incorporated within an unmodified vacuum chamber, and the sample is transferred automatically from SEM position to Raman position for correlative Raman-SEM analysis. For that purpose, SEM has to work at a low vacuum mode to avoid charging of nonconductive samples and to allow
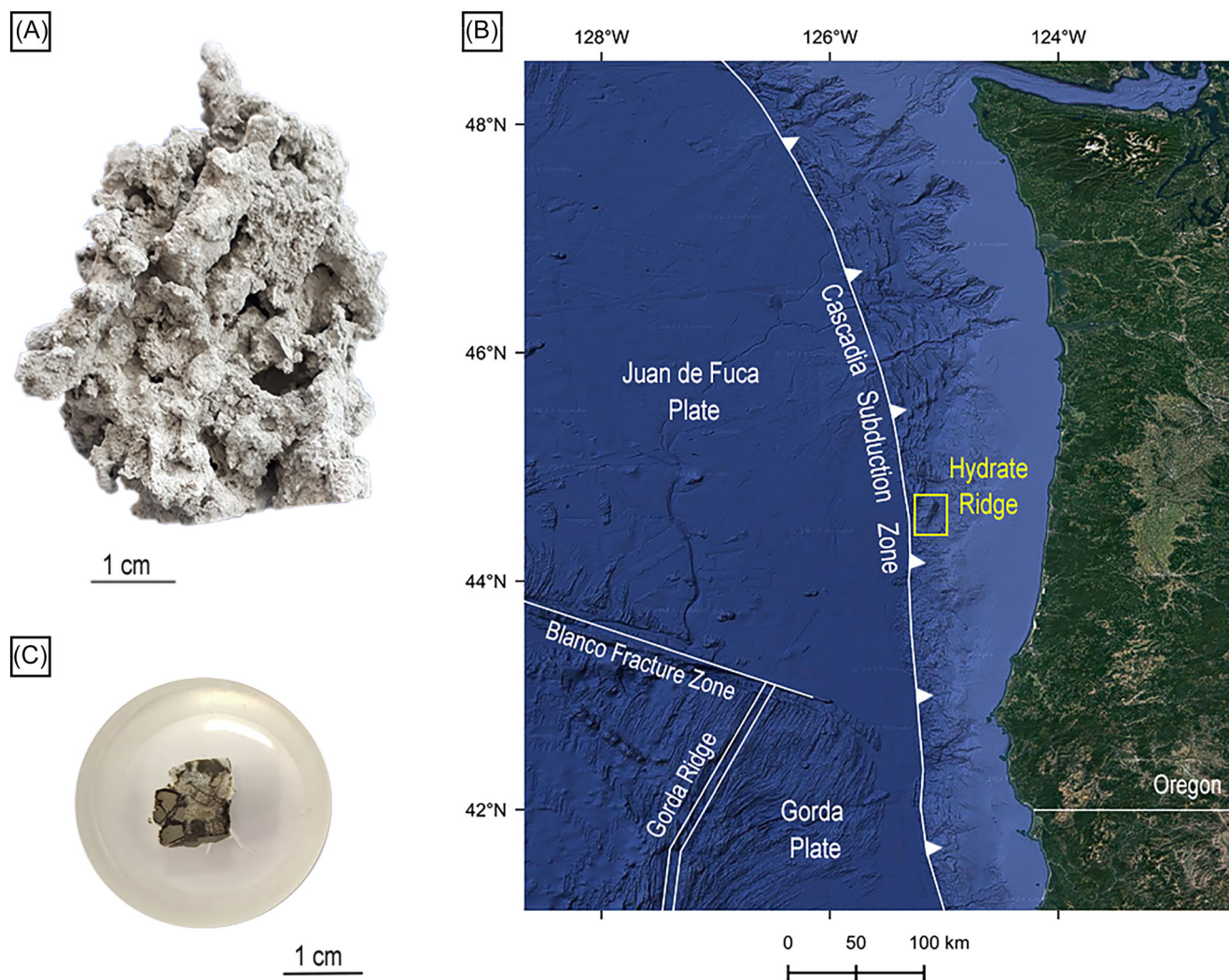

FIGURE 1 (A) Photograph of the clathrite rock sample. (B) The location of Hydrate Ridge in the Cascadia subduction margin. (C) Selected fragment of the clathrite sample embedded for SEM-Raman analysis.

Raman measurements. The instrument is detailed described in ref. 35.

The working method followed for the characterisation of the clathrite fragment consisted of five steps: (1) We acquired a secondary electron image (SE) for topology surface using C2D detector and a backscattered electron image (BSE) for compositional contrast through HDAsB detector. Both SEM images were taken at a working distance around 8.7 mm. (2) We used Aztec software to perform EDXS elemental mappings and to interpret the results. The aims of this step were twofold: to identify points and areas of interest for subsequent Raman analysis and to ease the interpretation of Raman spectra. (3) After a preliminary examination with the SEM, we transferred the clathrite fragment from SEM to Raman position and focused onto the sample. After that, an optical image was taken using a $100\times$ Raman objective lens (NA = 0.75) and overlaid onto BSE imaging in order to obtain correlative Raman spectra. Raman measurements and pre-processing were carried out through the WITec Control FIVE software. The Raman laser wavelength was 532 nm and the laser power, the exposure time and the number of accumulations were adjusted to avoid sample damage. (4) Clathrite fragment was then returned to SEM position to capture magnified SE images of the minerals of interest. (5) The Raman spectra taken were analysed by OriginPro 2022b software. The Raman peak positions, shifts, and full width at half maximum (FWHM) were determined using the Gaussian-Lorentzian curve-fitting.

In addition, we used a confocal Raman microspectrometer (Horiba LabRam HR Evolution spectrometer, Jobin Yvon Technology) in Centro de Investigaciones Energéticas, Medioambientales y Tecnológicas (CIEMAT) in Madrid. We characterised textures other than that of the minerals identified in the clathrite sample so as to determine by comparison whether the Raman signals obtained in both cases are diagnostic of mineral precipitation or biomediated conditions.

## 3 | RESULTS AND DISCUSSION

We focused the study on analysing calcium carbonate minerals that would be directly linked to the clathrate hydrate formation and dissociation processes, as well as the other possible associated opaque minerals (sulphides, oxides etc.) that could not yet be labelled by optical microscope. X-ray diffractograms of the clathrite sample revealed the presence of aragonite, Mg-calcite, quartz and chlorite-serpentine.[21] For the purpose of this study, the characterisation of the silicious breccia clasts formed by the process of dissociation of clathrate hydrates was not addressed.

Aragonite ($CaCO_3$) constitutes the main mineral phase of the clathrite sample (Figure S1a). It was identified by four intense Raman band positions[36] related to the translational and librational lattice mode between calcium and CO_3^{2-} group at 154 and 207 cm^{-1}, respectively, the ν_4 double degenerate in-plane bending of CO_3^{2-} group at 702 and 707 cm^{-1}, and the ν_1 symmetric stretching mode of CO_3^{2-} group at 1086 cm^{-1} (Figure S1b). We also detected seven additional weak lattice vibrational modes[37] near 144, 182, 192, 215, 249, 261 and 287 cm^{-1}. No variations of the Raman band parameters are observed throughout the direction of maximum crystal elongation. SEM images of those aragonite crystals show that they present an acicular habit and an arrangement in botryoidal aggregates (Figure S1c).

We detected some aragonites by the presence of a band at 207 cm^{-1} which, if not present, would match with that Raman signature of the magnesium-rich calcite. The shift of calcite Raman bands at higher wavenumbers indicates the substitution of Ca^{2+} ion by Mg^{2+} ion[38] (Figure S2). Thus, Mg-calcite bands detected at 154, 287, 712 and 1090 cm^{-1} correspond in this order to the translational and librational lattice mode, the ν_4 in-plane bending of CO_3^{2-} group and the ν_1 symmetric stretching mode of CO_3^{2-} group. The non-detection of the weak lattice vibration modes of aragonite and the doublet bands for ν_4 would suggest that aragonite was being replaced by Mg-calcite.[39]

The analysis of the SEM elemental mapping image show several carbonate grains with a zonation pattern related to a marked increase of Mg content towards the centre (Figure 2A). Raman spectroscopy analysis identified aragonite, Mg-calcite and dolomite as the minerals involved in the enriched magnesium chemical gradient (Figure 2B). Aragonite crystals form the outer mineral zone, and they are surrounding a Mg-calcite grain $(Ca,Mg)CO_3$, which in turn encloses a dolomite $CaMg(CO_3)_2$ grain. Dolomite was recognised by the external lattice vibrational modes at 178 and 302 cm^{-1}, and internal modes 726 and 1099 cm^{-1} corresponding to the ν_4 in-plane bending of CO_3^{2-} group and the ν_1 symmetric stretching mode of CO_3^{2-} group, respectively.[40]

The origin of the zoning pattern would be directly associated with the process of clathrate hydrate formation and dissociation. According to the ^{18}O isotopic results of clathrite published by Bohrmann et al.,[17] the precipitation of aragonite ($+3.68‰$) would be coetaneous with clathrate hydrate deposit formation, whereas Mg-calcite ($+4.86‰$) would postdate the dissociation of clathrate hydrates, owing to clathrate hydrates produce a hydrogen and oxygen isotope fractionation of pore-water by selecting the heavy isotopes, D and ^{18}O, for the formation of their structures.[41] If they dissociate, pore-water
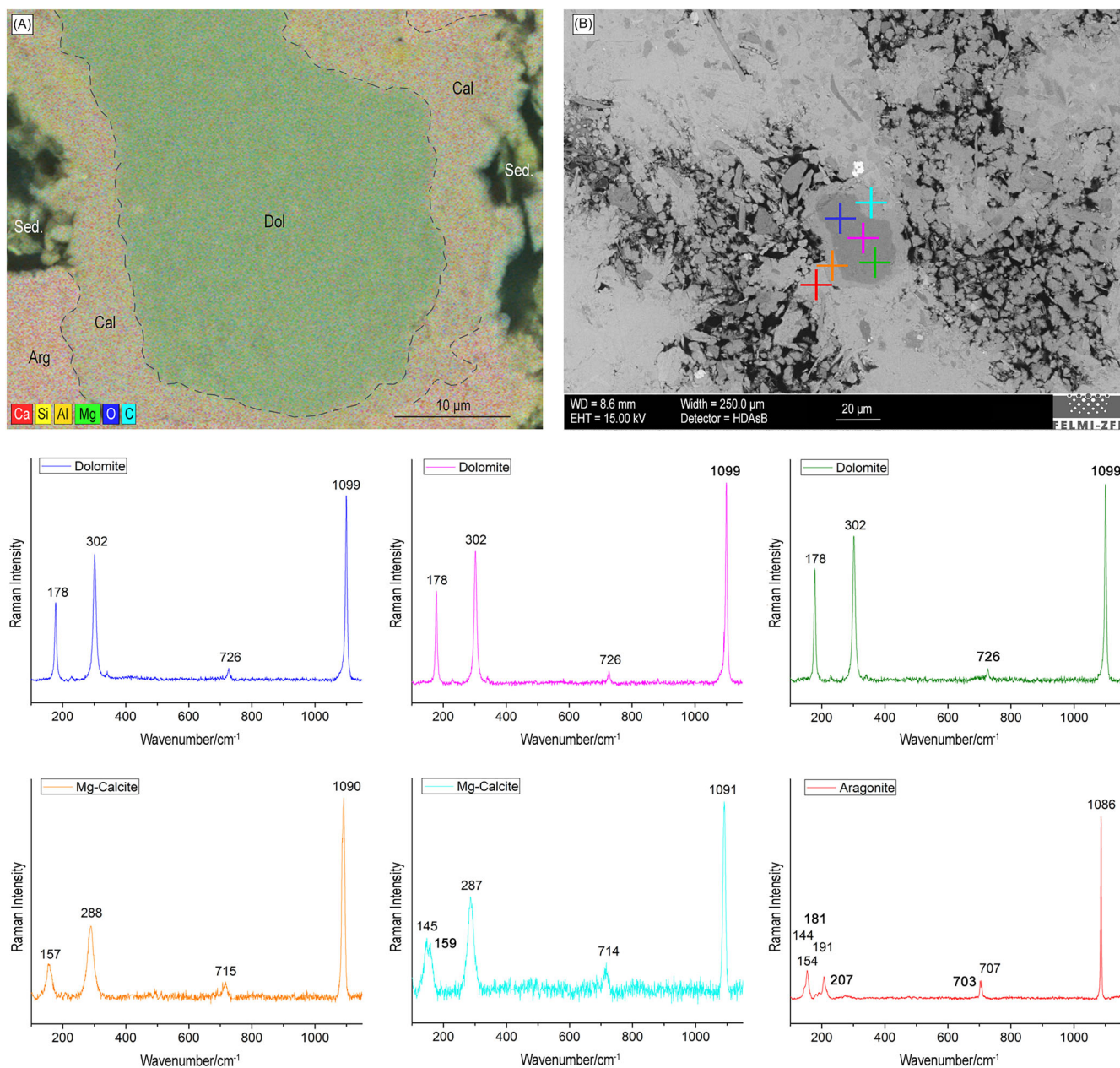
FIGURE 2 (A) EDX map shows an increasing gradient of Mg content towards the centre of the zoning pattern surrounded by brecciated silicate clasts (Brec). The minerals involved are aragonite (Arg), Mg-calcite (Cal), and dolomite (Dol). (B) Each coloured Raman spectrum refers to a point of the mineralogical zonation in the BSE image.

would become isotopically heavier and the Mg-calcite precipitates enriched in ^{18}O because part of these heavy ^{18}O atoms would be incorporated into its carbonate ions.[17,42] Hence, the calcite grain observed would be circumscribed to the space that must have been occupied by clathrate hydrates bordered by syn-precipitated aragonite crystals. Nevertheless, the ^{18}O enrichment is not plotted in the Raman signals of Mg-calcite analysed in this study. The intensity of ν_1 ($C^{16}O_3^{2-}$) band should have diminished by the appearance of new peaks near 1065 cm^{-1} and lower wavenumbers corresponding to the carbonate

groups[43] containing ^{18}O, $C^{16}O_2^{18}O^{2-}$, $C^{16}O^{18}O_2^{2-}$ and $C^{18}O_3^{2-}$. The explanation would rest on the fact that the concentration of the heavy oxygen isotope in the carbonate groups of the Mg-calcite would not be high enough to be reflected in its Raman spectrum. Culminating in the determination of the mineral sequence, dolomite precipitation may have preceded clathrate hydrate dissociation and, consequently, Mg-calcite precipitation because dolomite-calcite boundaries are well defined.

The crystalline degree of carbonate minerals would support the aforementioned precipitation sequence. The

crystallinity index was calculated from the ratio of the full width at half maximum (FWHM) of the ν_1 Raman symmetric stretching peak. Aragonite has the highest crystalline structure due to its low FWHM values ranging between 2.06 and 3.45. Similar FWHM values have been obtained for aragonites sampled at other active cold-seep sites, such as those on the Formosa Ridge in the South China Sea where gas hydrate reservoirs have also been identified and drilled.[44,45] Dolomite follows with 5.60–6.01, as the FWHM values for Mg-calcite are roughly 10. Mg-calcite, the carbonate likely formed from released methane, would precipitate with less crystalline structure due to the environmental instability induced by clathrate hydrates dissociation.

The spatial relationship between Mg-calcite and its dolomite host would imply that the dolomite grain might have formed into the pores of clathrate hydrates. The presence of dolomite would constitute a fossil record of clathrate hydrate microbiomes at Hydrate Ridge, based on previous studies on microdolomite mineralization within clathrate hydrate microbiomes in the Joetsu Basin discovered by Snyder et al.[24] Therefore, dolomite would become a potential mineral biosignature that could be preserved within the clathrite structure.

Correlative SEM images and Raman spectra revealed clusters of framboidal pyrite crystals, FeS_2, distributed around aragonite aggregates (Figure S3). Pyrite was identified by the two intense Raman peaks near 340 and 375 cm^{-1}, belong to S_2 liberation and in-phase S-S stretching vibrations.[44] The weak Raman band of coupled liberation/stretch modes near 430 cm^{-1} is not observed.[46,47]

Framboidal pyrites have been also documented as potential biosignatures. Works such as MacLean et al.[48] and Wacey et al.[49] reported different evidence for the presence of organic material within the pyrite microcrystals of a single framboid and highlighted the role of bacterial biofilm (e.g., sulphate-reducing bacteria) in the nucleation of pyrite microcrystals. Besides, Carrizo et al.[21] found lipid biomarkers of sulphate-reducing bacteria in a clathrite sample of the same location than the one that we have characterised in this work.

To ensure the signature of biological interaction in the Raman spectra of the framboidal pyrites, three abiotic massive pyrites from Mina de Las Cruces in Sevilla and other one from Mina de Cala in Huelva were investigated as examples of this other different origin. We found that the Raman signals of framboidal pyrites are slightly shifted to lower wavenumbers with regard to massive pyrites (Table 2). On the other hand, Raman signature of framboidal pyrites is concordant with that of pyrite-mineralised microfossils pods.[50] However, analytical studies of abiotically synthesised microspheres[44] and nanorods[51] pyrites under hydrothermal conditions in the laboratory have the same Raman peak positions as framboidal and biogenic pyrites (Table 2). Massive pyrite precipitates have a higher degree of crystallinity than the framboidal pyrites in this study, particularly with regard to the E_g mode at 340–346 cm^{-1}. Therefore, according to these results, we consider that Raman spectra of framboidal pyrites could be a geosignature of their crystallinization conditions and that a detailed biochemical analyses would be necessary to assess the biological influence on their origin.

Pyrites are not the only opaque minerals in the sample. Figure S4 shows a triangular shaped grain composed of several nanoparticles. The Raman spectrum characterises it as magnetite $Fe^{2+}Fe^{3+}_2O_4$. Nevertheless, Raman

TABLE 2 Relationship between textures and Raman band positions of the pyrites analysed in this study and published works.

Study	Texture	E_g mode (cm^{-1})	FWHM	A_g mode (cm^{-1})	FWHM	$T_g(3)$ mode (cm^{-1})	FWHM
Clathrite	Framboidal	340	9.85	374	11.60	-	-
		343	11.52	378	11.85	-	-
		340	8.63	376	10.04	-	-
Mina de Cala	Massive	346	1.70	383	1.85	435	5.04
		346	1.80	380	11.18	432	4.16
		345	2.47	381	5.37	432	4.69
Mina de Las Cruces		345	1.22	382	3.63	433	5.14
Wacey et al. (2021)	Microfossils pods	343	-	378	-	435	-
Wu et al. (2015)	Microspheres (synthetic)	342	-	377	-	429	-
Morales-Gallardo et al. (2016)	Nanorods (synthetic)	340	-	377	-	426	-

bands assigned to symmetric and asymmetric bends of O and Fe (at ~576 cm^{-1}) and symmetric stretch of O in Fe-O bonds (at ~692 cm^{-1})[52] are shifted to higher wavenumbers and are broader regarding Raman spectrum reference of magnetite published in the RRUFF database.[53] The cause of this displacement is unknown and could be due to several reasons such as the incorporation of some elements into the crystal structure or putative biogenicity.

4 | CONCLUSIONS

Clathrites can be identified from Raman spectroscopy combined with micro-imaging and geochemical analytical techniques because textures linked to isotopic and elemental changes would record a genesis associated with clathrate hydrate formation and dissociation.

Terrestrial clathrites are mainly composed of aragonite and Mg-calcite and may even contain dolomite grains. From near IR observations, we may argue that potential clathrites from ocean worlds might have not only a calcium and magnesium carbonate composition but also sodium or even ammonium carbonates such as those detected on Ceres.[12,54]

Variations on the degree of crystallinity among rock-forming carbonate minerals might denote signs of past processes of clathrate hydrate formation and dissociation. Clathrate hydrate dissociation might cause disruptive precipitation conditions in carbonate minerals, as would be the case of Mg-calcite which shows a low-crystalline structure. The bio-mediation of dolomite was inferred in the Hydrate Ridge sample, qualifying it as a mineral biosignature through combining mineral characterisation and studies of arrangement of the clathrite-forming minerals. On the other hand, the association with sulphides and the Raman signature of framboidal pyrites is a geosignature of formation conditions leading to the precipitation of framboid-like microtextured crystals. In this case, biochemical analysis would be required to assess their biogenicity. To sum up, we confirm that the combination of textural and mineralogical measurements is necessary to determine the clathrite origin of carbonates in other planets while they provide geosignatures of clathrate hydrate formation and dissociation processes. We suggest that clathrites are target minerals for astrobiology helping on searching for biosignatures because of their biomarkers preservation capacity and the potential precipitation of biomediated phases such as dolomite.

AUTHOR CONTRIBUTIONS

Ana de Dios-Cubillas led the manuscript building, interpretation, discussion, and writing. **Olga Prieto-Ballesteros** conceived the original idea. **Ana de Dios Cubillas, Manfred Nachtnebel, and Harald Fitzek** processed and analysed the samples and interpreted the Raman spectra and the results of SEM. **Olga Prieto-Ballesteros, Manfred Nachtnebel, Harald Fitzek, and Hartmuth Schröttner** discussed and revised the manuscript.

ETHICS STATEMENT

This study does not contain any studies with human or animal participants conducted by any of the authors.

CONFLICT OF INTEREST STATEMENT

The authors declare no competing financial interest.

DATA AVAILABILITY STATEMENT

No new data were created in this study. Data sharing is not applicable to this article. These are scientific results derived from the geochemical analysis of natural rock samples using standard and universally known methods. The data are purely descriptive.

ORCID

Ana de Dios-Cubillas https://orcid.org/0000-0003-3787-7458

REFERENCES

[1] J. P. Kennet, B. Frackler-Adams, *Geology* **2000**, *28*, 215.

[2] G. Bohrmann, E. Suess, J. Greinert, B. Teichert, T. Naehr, *Proc. Fourth Int. Conf. Gas Hydrates* **2002**, 102.

[3] E. D. Sloan, C. A. Koh, *Clathrate hydrates of natural gases*, 3rd ed., CRC Press, New York **2007**.

[4] O. Prieto-Ballesteros, J. S. Kargel, M. Fernández-Sampedro, F. Selsis, E. S. Martínez, D. L. Hogenboom, *Icarus* **2005**, *177*, 491.

[5] A. Bouquet, O. Mousis, J. H. Walte, S. Picaud, *Geophys. Res. Lett.* **2015**, *42*, 1334.

[6] M. T. Bland, C. A. Raymond, P. M. Schenk, R. R. Fu, T. Kneissl, J. H. Pasckert, H. Hiesinger, F. Preusker, R. S. Park, S.

Marchi, S. D. King, J. C. Castillo-Rogez, C. T. Russell, *Nat. Geosci.* **2016**, *9*, 538.

[7] J. Carroll, *Natural gas hydrates: a guide for engineers*, 2nd ed., Elsevier, Burlington **2009**.

[8] V. Muñoz-Iglesias, *Efectos de la presión en la geoquímica de la corteza y del océano del satélite Europa*; Published Ph.D. Thesis, Universidad Complutense de Madrid, Madrid **2014**.

[9] S. W. Kieffer, X. Lu, C. M. Bethke, J. R. Spencer, S. Marshak, A. Navrotsky, *Science* **2006**, *314*, 1764.

[10] F. G. Carrozzo, M. C. De Sanctis, A. Raponi, E. Ammannito, J. Castillo-Rogez, B. L. Ehlmann, S. Marchi, N. Stein, M. Ciarniello, F. Tosi, F. Capaccioni, M. T. Capria, S. Fonte, M. Formisano, A. Frigeri, M. Giardino, A. Longobardo, G. Magni, E. Palomba, F. Zambon, C. A. Raymond, C. T. Russell, *Sci. Adv.* **2018**, *4*, e1701645. https://doi.org/10.1126/sciadv.1701645

[11] F. Postberg, S. Kempf, J. Schmidt, B. Brilliantov, A. Beinsen, B. Abel, U. Buck, R. Srama, *Nature* **2009**, *459*, 1098.

[12] S. De Angelis, C. Carli, F. Tosi, P. Beck, O. Brissaud, B. Schmitt, S. Potin, M. C. De Sanctis, F. Capaccioni, G. Piccioni, *Icarus* **2019**, *317*, 388.

[13] S. Kempf, U. Beckmann, J. Schmidt, *Icarus* **2010**, *206*, 446.

[14] P. H. Figueredo, R. Greeley, S. Neuer, L. Irwin, D. Schulze-Makuch, *Astrobiology* **2003**, *3*, 851.

[15] S. Rajput, N. K. Thakur, *Geological controls for gas hydrates and uin nconventionals*, Elsevier, Amsterdam **2016**.

[16] J. Greinert, G. Bohrmann, E. Suess, in *Natural gas hydrates: occurrence, distribution and detection, geophysical monograph*, (Eds: C. K. Paull, W. K. Dillon), American Geophysical Union, Washington D. C. **2001** 99.

[17] G. Bohrmann, J. Greinert, E. Suess, M. Torres, *Geology* **1998**, *26*, 647.

[18] E. A. Burtin, *Chem. Geol.* **1993**, *105*, 163.

[19] G. Aloisi, C. Pierre, J.-M. Rouchy, J.-P. Foucher, J. Woodside, *Earth Planet. Sci. Lett.* **2000**, *184*, 321.

[20] K. A. Campbell, *Palaeogeogr. Palaeoclimatol. Palaeoecol* **2006**, *232*, 362.

[21] D. Carrizo, A. de Dios-Cubillas, L. Sánchez-García, I. López, O. Prieto-Ballesteros, *Astrobiology* **2022**, *22*, 552. https://doi.org/10.1089/ast.2021.0036

[22] A. Boetius, K. Ravenschlag, C. J. Schubert, D. Rickert, F. Widdel, A. Gieseke, R. Amann, B. B. Jørgensen, U. Witte, O. Pfannkuche, *Nature* **2000**, *407*, 623.

[23] J. J. Middelburg, K. Soetaert, M. Hagens, *Rev. Geophys.* **2020**, *58*, e2019RG000681. https://doi.org/10.1029/2019RG000681

[24] G. T. Snyder, R. Matsumoto, Y. Suzuki, M. Kouduka, Y. Kakizaki, N. Zhang, H. Tomaru, Y. Sano, N. Takahata, K. Tanaka, S. A. Bowden, T. Imajo, *Sci. Rep.* **2020**, *10*, 1876. https://doi.org/10.1038/s41598-020-58723-y

[25] E. J. Schneider, J. C. Moore, H. Schwartz, E. Silver, in *Book of Abstracts, 2004 American Geophysical Union (AGU 2004)*, Montreal, Paper P21A-0203.

[26] C. Argentino, S. Conti, C. Fioroni, D. Fontana, *Geosciences* **2019**, *9*, 134. https://doi.org/10.3390/geosciences9030134

[27] K. C. Hester, R. M. Dunk, S. N. White, P. G. Brewer, E. T. Peltzer, E. D. Sloan, *Geochim. Cosmochim. Acta* **2007**, *71*, 2947.

[28] T. Leefmann, M. Blumenberg, B. C. Schmidt, V. Thiel, in *Spongy, slimy, cosy & more*, (Eds: F. Wiese, M. Reich Gernot Arp), Universitätsverlag Göttingen, Göttingen **2014**, 113.

[29] S. E. Jorge Villar, H. G. M. Edwards, *Anal. Bioanal. Chem.* **2006**, *384*, 100. https://doi.org/10.1007/s00216-005-0029-2

[30] M. F. C. Verkaaik, J.-H. Hooijschuur, G. R. Davies, F. Ariese, *Astrobiology* **2015**, *15*, 697. https://doi.org/10.1089/ast.2015.1329

[31] M. Baqué, T. Backhaus, J. Meeßen, F. Hanke, U. Böttger, N. Ramkissoon, K. Olsson-Francis, M. Baumgärtner, D. Billi, A. Cassaro, R. de la Torre Noetzel, R. Demets, H. Edwards, P. Ehrenfreund, A. Elsaesser, B. Foing, F. Foucher, B. Huwe, J. Joshi, N. Kozyrovska, P. Lasch, N. Lee, S. Leuko, S. Onofri, S. Ott, C. Pacelli, E. Rabbow, L. Rothschild, D. Schulze-Makuch, L. Selbmann, P. Serrano, U. Szewzyk, C. Verseux, D. Wagner, F. Westall, L. Zucconi, J.-P. P. de Vera, *Sci. Adv.* **2022**, *8*, 1. https://doi.org/10.1126/sciadv.abn7412

[32] M. Benito-Parejo, P. Rodríguez-Pérez, A. Marín, J. A. Rodríguez-Prieto, R. Canchal, A. Moral, F. Rull. *8th international conference on photonics, optics and laser technology*, PHOTOPTICS, Valletta, Malta **2020**, https://doi.org/10.5220/0008966701070113

[33] M. Adang, A. Ainabe, A. Dave, A. Dumitrescu, A. E. Engle, S. Lamm, C. Liou, S. Y. W. Low, C. McClelland, G. Miceli, P. Patel, P. Salazar, L. Su, J. Todd, A. Vigneron, B. Wylie, *AIAA SCITECH* **2023**, 1968. https://doi.org/10.2514/6.2023-1968

[34] E. Suess, M. E. Torres, G. Bohrmann, R. W. Collier, J. Greinert, P. Linke, G. Rehder, A. Trehu, K. Wallmann, G. Winckler, E. Zuleger, *Earth Planet. Sci. Lett.* **1999**, *170*, 1.

[35] R. Schmidt, H. Fitzek, M. Nachtnebel, C. Mayrhofer, H. Schroettner, A. Zankel, *Macromol. Symp.* **2019**, *384*, 1800237. https://doi.org/10.1002/masy.201800237

[36] G. Nehrke, J. Nouet, *Biogeosciences* **2011**, *8*, 3761.

[37] J. Urmos, S. K. Sharma, F. T. Mackenze, *Am. Mineral.* **1991**, *76*, 641.

[38] L. Borromeo, U. Zimmermann, S. Andò, G. Coletti, D. Bersani, D. Basso, P. Gentile, B. Schulz, E. Garzanti, *E. J. Raman Spectrosc.* **2017**, *48*, 983.

[39] J. E. Parker, S. P. Thompson, A. R. Lennie, J. Potter, C. C. A. Tang, *CrysEngComm* **2010**, *12*, 1590.

[40] S. Kraft, E. Knittle, Q. Williams, *J. Geophys. Res.* **1991**, *96*, 17997.

[41] A. Hachikubo, T. Kosaka, M. Kida, A. Krylov, H. Sakagami, H. Minami, N. Takahashi, H. Shoji, *J. Geophys. Res.* **2007**, *34*, L21502. https://doi.org/10.1029/2007GL030557

[42] G. Bohrmann, M. E. Torres, in *Marine geochemistry*, (Eds: H. D. Schulz, M. Zabel), Springer, Berlin **2006** 481.

[43] P. Gillet, P. McMillan, J. Schott, J. Badro, A. Grzechnik, *Geochim. Cosmochim. Acta* **1996**, *60*, 3471.

[44] S. Xi, X. Zhang, Z. Du, L. Li, B. Wang, Z. Luan, C. Lian, J. Yan, *J. Asian Earth Sci.* **2018**, *168*, 207. https://doi.org/10.1016/j.jseaes.2018.01.023

[45] S. Xi, X. Zhang, Z. Luan, Z. Du, L. Li, Z. Liang, C. Lian, J. Yan, *Minerals* **2019**, *9*, 751. https://doi.org/10.3390/min9120751

[46] J. Wu, Y. Liang, P. Bai, S. Zheng, L. Chen, *RSC Adv.* **2015**, *5*, 65575.

[47] J. Walter, X. Zhang, B. Voigt, R. Hool, M. Manno, F. Mork, E. S. Aydil, C. Leighton, *Phys. Rev. Materials* **2017**, *1*, 065403. https://doi.org/10.1103/PhysRevMaterials.1.065403

[48] L. C. W. MacLean, T. Tyliszczak, P. U. P. A. Gilbert, D. Zhou, T. J. Pray, T. C. Onstott, G. A. Southam, *Geobiology* **2008**, *6*, 471.

[49] D. Wacey, M. R. Kilburn, M. Saunders, J. B. Cliff, C. Kong, A. G. Liu, J. J. Matthews, M. D. Brasier, *Geology* **2015**, *43*, 27.

[50] D. Wacey, K. Eiloart, M. Saunders, *Chem. Geol.* **2021**, *581*, 120419. https://doi.org/10.1016/j.chemgeo.2021.120419

[51] M. V. Morales-Gallardo, A. M. Ayala, M. Pal, M. A. Cortes Jacome, J. A. Toledo Antonio, N. R. Mathews, *Chem. Phys. Lett.* **2016**, *660*, 93.

[52] O. N. Shebanova, P. Lazor, *J. Solid State Chem.* **2003**, *174*, 424.

[53] B. Lafuente, R. T. Downs, H. Yang, N. Stone, in *Highlights in mineralogical crystallography*, (Eds: T. Armbruster, R. M. Danisi), W. De Gruyter, Berlin **2015** 1.

[54] M. C. De Sanctis, A. Raponi, E. Ammannito, M. Ciarniello, M. J. Toplis, H. Y. McSween, J. C. Castillo-Rogez, B. L. Ehlmann, F. G. Carrozzo, S. Marchi, F. Tosi, F. Zambon, F. Capaccioni, M. T. Capria, S. Fonte, M. Formisano, A. Frigeri, M. Giardino, A. Longobardo, G. Magni, E. Palomba, L. A. McFadden, C. M. Pieters, R. Jaumann, P. Schenk, R. Mugnuolo, C. A. Raymond, C. T. Russell, *Nature* **2016**, *536*, 54. https://doi.org/10.1038/nature18290

SUPPORTING INFORMATION

Additional supporting information can be found online in the Supporting Information section at the end of this article.